Surface orientation dependent interaction of cobalt (II) precursors with alpha-alumina

Céline Chizallet, Christian Schlaup, Emiliano Fonda, Xavier Carrier

Surface orientation dependent interaction of cobalt (II) precursors with alpha-alumina

Céline Chizallet,[1,] Christian Schlaup,[2] Emiliano Fonda,[3] Xavier Carrier[2,*]*

[1] IFP Energies nouvelles, Rond-point de l'échangeur de Solaize, BP3, 69360 Solaize, France

[2] Sorbonne Université, CNRS, Laboratoire de Réactivité de Surface, LRS, F-75005 Paris, France

[3] Synchrotron SOLEIL, L'Orme des Merisiers, Saint Aubin BP 48, F-91192 Gif S Yvette, France

Corresponding authors : celine.chizallet@ifpen.fr ; xavier.carrier@sorbonne-universite.fr

ABSTRACT.

The performances of alumina-supported cobalt catalysts strongly depend on Co/alumina interactions, that are poorly understood. In the present work, α-alumina surfaces are used as models of polycrystalline support, to unravel their orientation dependent behavior by GI-EXAFS. The Co^{II}/ α-alumina interactions in the dried state are investigated, with a resolution of the parallel *versus* perpendicular deposit formation. DFT calculations shed light on the existence of specific grafting modes. EXAFS shows that $Co(OH)_2$ forms parallel to the R($1\bar{1}02$), A($11\bar{2}0$) and M($10\bar{1}0$) surfaces, whatever the contact time (from 1 hour to 6 days). However, a specific behavior of the C(0001) surface is observed. Whereas after one hour, the same parallel $Co(OH)_2$ is observed, at longer times it disappears while species exhibiting long then short Co-Co distances appear. The latter is assigned to epitaxial grafting of Co^{II} leading to a mixed phase, that is possible parallel to the C surface due to surface symmetry.

KEYWORDS.

GI-EXAFS, density functional theory, cobalt, alpha-alumina, grafting

1. INTRODUCTION

Cobalt-based catalysts are widely used at the industrial scale for many large-scale energy-related processes. Among these, hydrotreating[1] and Fischer-Tropsch[2, 3] are the main Co consumers in heterogeneous catalysis. Oxygen evolution reactions [4, 5] and many conversion reactions of short hydrocarbons also make use of cobalt catalysts[6-8]. In all cases, a careful control of the cobalt environment, particle size and dispersion is key in order to derive structure activity relationships needed for a rational development of improved catalytic formulations. As a matter of fact, the effect of cobalt particle size has been largely debated in Fischer-Tropsch (FT) where it was initially believed that FT is a structure insensitive reaction [2]. However, de Jong and coworkers [9, 10] later showed that activity and selectivity drop for Co particles smaller than 6-8 nm in model carbon-supported catalysts which was explained by the blocking of undercoordinated sites (edges/corners) as well as a low reactivity of terraces. Deactivation of FT catalysts is also strongly influenced by the Co particle size [11] and distribution [12]. For particles below about 5 nm, Co is reoxidized in reaction conditions which leads to the formation of an inactive surface cobalt aluminate.

A careful control of the cobalt particle size and Co environment can only be achieved through a molecular-scale understanding of the operation parameters during the preparation of the catalyst. In this respect, and in the frame of the present Special Issue, it has to be underlined that the work of Michel Che was pioneer in considering the interfacial chemistry at the solid/liquid interface as the key starting point for a rational design of heterogeneous catalysts [13]. As for Co-based catalysts, he showed that a systematic description of the Co speciation at the oxide/water interface during Co deposition is a crucial prerequisite to understand and control the formation of inactive cobalt aluminate species upon thermal treatment and Co particles upon reduction [14]. Related molecular-scale approaches by other groups were reviewed by Bourikas et al. [15] and the role of the support was also shown to be

central for a full description of the Co sorption mechanism: silica for example was recognized to favor the formation of $Co(OH)_2$-like precipitates while TiO_2 promotes the formation of surface complexes. Surface precipitates were also identified on γ-alumina but they were assigned to hydrotalcite-like Co/Al phases formed by alumina dissolution [16, 17].

In a practical context, alumina supports are widely used despite the formation of these Co/Al phases and of the presence of poorly reducible species, thus in the present work, we focus our attention on alumina supported cobalt catalysts. For these systems, metal-support interactions where shown to have a direct role on metal distribution and in the end on the catalytic activity, selectivity and stability[18-22]. Understanding the interaction modes of the cobalt precursor with the surface of alumina is thus a prerequisite for the optimization of the performances.

Model approaches were also developed in order to better describe the role of the support on Co sorption, namely for alumina, using oriented single crystals of α-alumina with the predominant C(0001) and R($1\bar{1}02$) orientations [23, 24]. In both cases, EXAFS characterization revealed the formation of isolated surface complexes while no sign of surface precipitation was observed. Another type of model approach was provided by density functional theory (DFT) works, that appears to be a powerful approach to better define the coordination modes and strength of metallic compounds on inorganic surfaces, in particular in the case of cobalt supported on alumina [25-27]. Larmier et al. [25] studied the genesis of a surface $Co(OH)_2$ phase on two different surfaces of γ-alumina, the predominant (110) and (100) facets. The incipient formation of $Co(OH)_2$ is shown to be directed by a strong epitaxial relationship between the surface phase and the alumina facets.

This work aims at broadening the latter approaches on the support effect at the experimental and theoretical level by considering the adsorption mechanism of Co^{2+} on four different α-alumina surface orientations : A($11\bar{2}0$), C(0001), M($10\bar{1}0$) and R($1\bar{1}02$) that have

been used before as surrogates for mimicking the reactivity of γ-alumina facets, the archetypal catalyst support but that is not available as single crystal wafers [28, 29]. These previous works showed a support-dependent adsorption for Mo [28, 29] and Ni [30] which needs to be evaluated for Co in order to assess a potential surface-dependent adsorption mechanism on γ-alumina nanoparticles. Grazing-incidence EXAFS at the Co K-edge is used to probe the local structure of adsorbed Co at the dried state and these results are discussed in the light of periodic DFT calculations performed for each corresponding surface orientation. A surface-orientation dependent behavior is observed, that opens perspectives in the control of the nature of the surface deposits as a function of the surface symmetry and hydroxyl group nature.

2. EXPERIMENTAL SECTION AND METHODS

2.1. Sample preparation

Electrolyte preparation

All electrolyte solutions were prepared using analysis grade chemicals and ultra-pure water (MilliQ®, Merck Millipore, 18.2 MΩ cm). In order to minimize intrusion of carbon dioxide, all electrolytes were deaerated with nitrogen for at least 1 hour before utilization.

Alumina sample preparations

Commercially available α-alumina single crystals (SurfaceNet, Germany) with four different orientations: A($11\bar{2}0$), C(0001), M($10\bar{1}0$) and R($1\bar{1}02$) with dimensions of Ø 50 × 0.5 mm (misorientation < 0.1°) were used for all measurements.

Before utilization they were chemically cleaned and calcined. The chemical cleaning was conducted by immersing them subsequently into MilliQ water, diluted HNO_3 (pH = 2.0), MilliQ water; diluted NH_3 (pH = 9.0), and MilliQ water, each for 30 minutes, respectively.

The subsequent calcination lasted 14 hours at a temperature of 700 °C in air in a muffle furnace.

Cobalt adsorption

Cobalt adsorption was performed by immersing the alumina single crystals into a $Co(NO_3)_2$ solution ($c = 1 \cdot 10^{-3}$ mol•L^{-1}) with a pH = 8.5 (adjusted with a $20 \cdot 10^{-3}$ mol•L^{-1} KOH solution). The choice of the base has little influence since no adsorbed potassium was found with XPS for all samples studied. After an adsorption time of 1 hour, 1 day, or 6 days, respectively, the samples were removed from the solution and excessive electrolyte was removed in a dry nitrogen stream at room temperature. The ***washed*** samples were immersed subsequently into MilliQ water for about 10 minutes and dried under nitrogen.

Quantification of adsorbed cobalt was conducted with XPS using the Co_{2p} signal (Figure S1), following the method detailed before [31]. Results are shown in Figure 1 as a function of final pH for three different adsorption times (1 hour, 1 day and 7 days). Results for 6 days are very close to 7 days. Co quantification yields results ranging from 1.4 to 4.5 Co atoms.nm^{-2} which would yield weight loadings of 2.7 to 8.1 wt% Co on a conventional γ-Al_2O_3 of 200 m^2.g^{-1}.

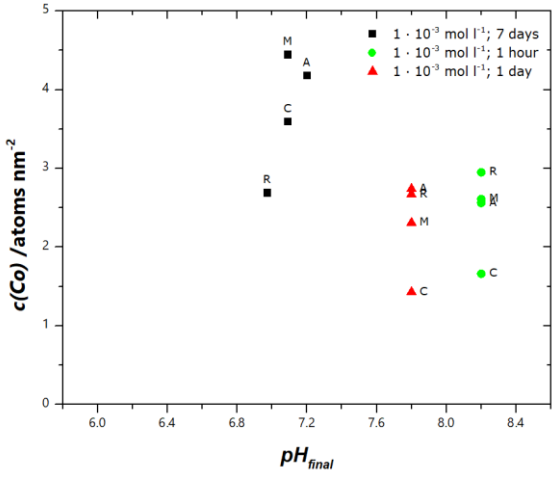

Figure 1. Cobalt adsorption on the four crystal orientations (A(11$\bar{2}$0), C(0001), M(10$\bar{1}$0) and R(1$\bar{1}$02)) as a function of final pH (starting pH is 8.5). Three sets of data are shown corresponding to different adsorption times: 1 hour (green), 1 day (red) and 7 days (black).

It has to be noted that in our experimental conditions ($[Co^{2+}] = 1 \bullet 10^{-3}$ mol$\bullet L^{-1}$, initial pH = 8.5), no homogeneous precipitation of $Co(OH)_2$ was visually detected in the impregnation solution. Nevertheless, thermodynamic calculations reported by Towle et al [32] show that the solution is supersaturated with respect to $Co(OH)_2$ precipitation in our initial conditions but undersaturated at the final pH (about 7) of long-term experiments (6/7 days). No measurable Co sorption was observed for a final pH below 6.5.

2.2.XAS measurements

Grazing-Incidence XAS measurements (XANES and EXAFS) at the Co K-edge were conducted on the SAMBA beamline [33] of the Soleil synchrotron facility. The beamline was equipped with a Si220 sagittal bending monochromator and a pair of Pd coated mirrors set at an incidence of 6 mrad. Mirrors were used to vertically collimate X-ray beam (1^{st} mirror) and vertically focus radiation closer to sample (2^{nd} mirror placed after monochromator) and for harmonic rejection. Nitrogen/Helium filled ionization chambers were used for monitoring X-ray flux, while X-ray fluorescence emitted by the sample was measured with a solid state energy resolved HPGe multi pixel detector (monolithic 36 pixels Canberra) coupled to XIA DxMap digital signal processors.

Samples have been loaded on a triple axis goniometer to align their surface parallel to the incident radiation electric field or perpendicular, while keeping the ability to rotate them and aligning at close to grazing incidence. Measurements have been optimized in total reflection at an incidence angle of 0.25°. Data have been measured in fluorescence mode.

The setup was specially designed for the experiment for short adsorption times (1 hour) that were conducted in-situ (i.e. on the beamline) : up to two plastic Beakers containing different solutions (cobalt solutions or water) were put on a translator. The sample could be automatically immersed and removed from any solution at a speed of 0.1mm/s ensuring that

any drops were left on the surface. Thus measurements could be remotely sequenced at each preparation step (adsorption and washing) and at different incidence angle between two extreme light polarization orientations (parallel and perpendicular to the surface). The fluorescence detector was able to vertically translate to avoid shadowing from the sample when in parallel orientation (sample nearly parallel to ground) and avoid too grazing emergence position. For each polarization multiple spectra were acquired and averaged. Incidence angles were optimized for maximum intensity and adjusted to avoid substrate Bragg reflections that considerably complicate data acquisition.

EXAFS data were processed using the Demeter software package with FEFF6 theoretical standards [34].

2.3. DFT calculations

Methods

Periodic density functional theory (DFT) calculations were performed using a plane-wave method as implemented in the Vienna Ab initio Simulation Package [35, 36]. The exchange-correlation functional was treated within the generalized gradient approximation (GGA) parameterized by Perdew, Burke and Ernzerhof [37] (PBE). The D2 correction of Grimme [38, 39] was applied to account for long-range dispersion interactions. The electron-ion interaction was described by the projector augmented wave (PAW) scheme [40] with an energy cutoff of 400 eV. Spin-polarized calculations were performed (cobalt (II): d^7 electronic configuration) and used the interpolation formula of Vosko, Wilk and Nusair [41]. Following the analysis of experimental UV-visible spectra [42] (according to Tanabe-Sugano diagrams), cobalt atoms were considered in their high-spin state (quartet). With several complexes in the cell, the spin coupling was taken as ferromagnetic. It was indeed shown that in β-$Co(OH)_2$, a ferromagnetic coupling exists in the layers, while it is antiferromagnetic between those layers

[43]. Gaussian smearing with σ = 0.05 eV was used. The criterion for the convergence of the self-consistent cycles was set to 10^{-6} eV. Geometry optimizations were run until forces on relaxed atoms were lower than 2.10^{-2} eV.Å^{-1}. All calculations were performed at the Γ-point.

Surface models

The four surface orientations considered experimentally were investigated computationally (Figures 2 and S2). Multiple cells were considered each time to allow the simulation of low cobalt coverage. So as to mimic a strongly hydrated case, surface Al atoms were saturated by hydroxylation.

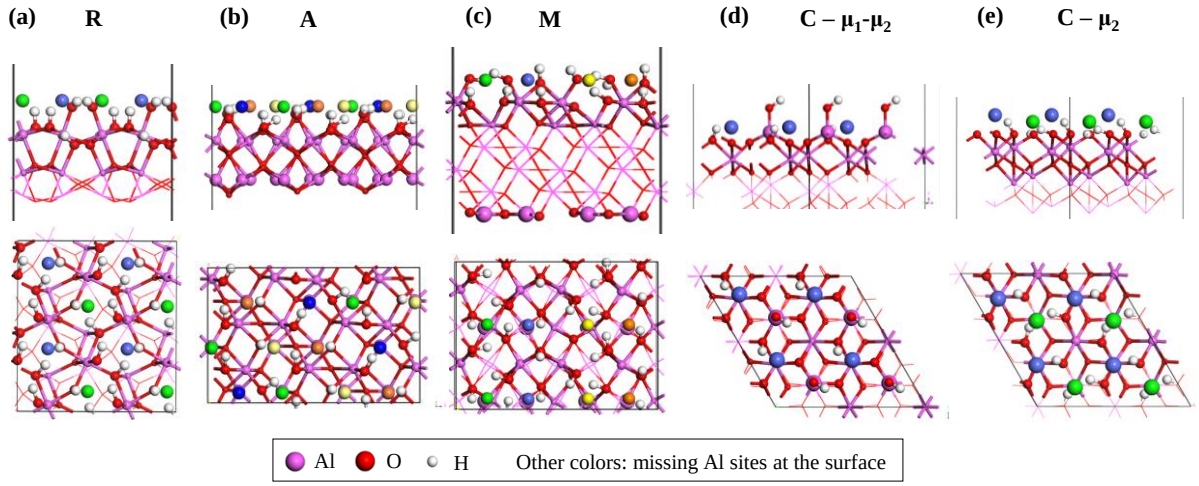

Figure 2. Side (top) and top (bottom) views of surface models considered in the present work, with depiction of the missing cationic sites at the surface, expected to be preferred sites for epitaxial growth. Non-equivalent sites are depicted by different colours. (a) R surface, (b) A surface, (c) M surface, (d) and (e) C surfaces. For side views, only the outermost layers are depicted for the sake of clarity. Full sides views can be found in Figure S2.

For the R surface, the termination proposed by Trainor et al. [44], simulated by Tougerti et al.[45] with θ_{OH} = 23.9 nm^{-2}, was used as a starting point, knowing that the surface symmetry would remain the same if one would consider other kinds of terminations (such as the one called C2 in ref. [45]).

The M (θ_{OH} = 19.4 nm^{-2}) and A (θ_{OH} = 16.8 nm^{-2}) models were taken from ref. [31] but the lateral dimensions of the cells were adapted (M: 9.52x12.99 Å², A: 8.24x12.99 Å²) so

as to allow a gradual investigation of the coverage with cobalt. The initial OH coverages are 19.4 (μ_1, μ_2, μ_3-OH, adsorbed water molecules) and 16.8 (μ_1, μ_2, μ_3-OH) OH.nm^{-2} for the M and A surfaces respectively.

Two types of hydroxylated 2x2 surface models were considered for the C orientation [46, 47]. The first one exhibits μ_2-OH only (24.3 OH.nm^{-2}), the second combines μ_1-OH and μ_2-OH (16.2 OH.nm^{-2}). This choice is motivated by the conditions that we wish to simulate (after drying at room temperature at least).

Interaction with Co^{II}

Standard Gibbs free energy of adsorption $\Delta_r G°_{ads}$ given by cobalt atom, corresponding to the chemical reaction depicted by equation 1, was quantified at 298 K by the method proposed in ref. [25] .

$$\text{Alumina}_{surf} + m\ Co(OH)_2(H_2O)_2 = \text{Alumina-m-Co}_{surf} + n\ H_2O \qquad \text{Eq. (1)}$$

The reference cobalt complex was $Co(OH)_2(H_2O)_2$. Indeed, in the framework of the periodic boundary conditions calculations undertaken here, energetics cannot be accurately determined for charged systems. Moreover, within this constraint, the optimization of an isolated octahedral complex ($Co(OH)_2(H_2O)_4$) led to the decoordination of two water molecules from Co. For the evaluation of the Gibbs free energy of adsorption of the cobalt complex, we assume that the temperature dependence of the internal energies is due to the desorbed water molecules only and that the entropy difference of the surface with or without an adsorbed complex is zero, so that entropic terms are hold by water only.

3. RESULTS AND DISCUSSION

Co deposition on the four different α-alumina orientations, A($11\bar{2}0$), C(0001), M($10\bar{1}0$) and R($1\bar{1}02$), was followed with XAS as a function of the deposition time (1 hour, 1 day or 6

days). Short time experiments (1 hour) were conducted "*in situ*" as explained in the experimental section, i.e. the immersion of the wafer in the Co solution (and a following washing step in some cases) were automatically realized on the beamline with a motorized arm in order to avoid any delay between the experiment and the characterization. Long time experiments (1 or 6 days) were realized right before the XAS experiments. Results obtained on the R($1\bar{1}02$) plane will be detailed first. Then, DFT results will be discussed in line with these results, analyzing the relevance of the description of the observed phenomena in terms of grafting. The finding are then generalized for the other investigated surfaces, with a specific behavior of the C surface.

3.1. Behavior of the R surface

EXAFS Fourier Transform (FT) (Figure 3) of Co(II)/α-Al_2O_3 on the R ($1\bar{1}02$) plane show two peaks after 6 days of Co adsorption that are assigned to Co-O and Co-Co neighbors. Results of the fit are given in Table S1. The close similarity of the Fourier-Transform in parallel polarization with that of $Co(OH)_2$ (a lamellar brucite-type structure) clearly indicates surface precipitation of the latter on the R($1\bar{1}02$) plane. Notably, as mentioned in section 2.1, no homogeneous precipitation is expected in the present experimental conditions, so that the observed $Co(OH)_2$ phase is likely connected to the surface at some point. The Co-O (2.08 Å) and Co-Co (3.17 Å) distances are fully consistent with that for $Co(OH)_2$ (2.10 Å and 3.17 Å [32]). Such precipitation (Co^{2+} + 2 OH^- = $Co(OH)_2$) is also in line with the large drift of pH from the initial value of 8.5 to a final value close to 7 for long adsorption times (Figure 1). Polarization-dependent spectra can yield another key information on a potential surface-dependent precipitation of the supported Co phase by comparing the spectra when the electric field vector of the synchrotron beam is set parallel or perpendicular to the surface of the single crystal wafer [30]. In the present case, the near absence of a Co-Co contribution in

perpendicular polarization strongly suggests that the surface precipitation of $Co(OH)_2$ occurs mostly parallel to the surface, i.e the basal (001) plane of the brucite structure is aligned with the surface. The same phenomenon was previously described for the surface precipitation of Ni hydroxide on the same R ($1\bar{1}02$) surface [30].

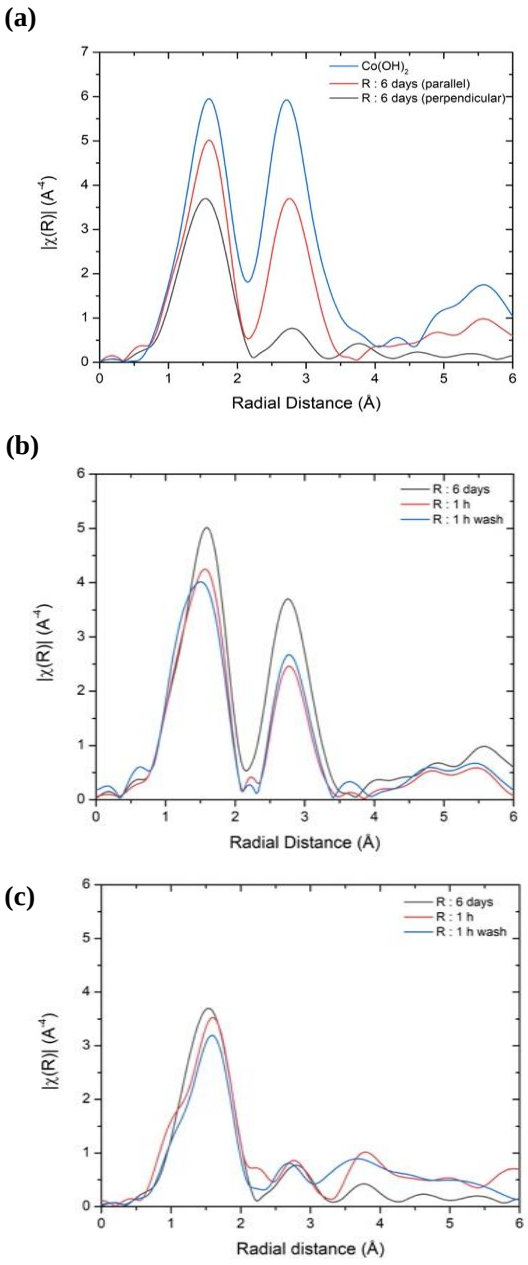

Figure 3. Fourier transforms (Δk = 3-8.5 $Å^{-1}$) uncorrected for phase shift of k^3-weighted Co K-edge EXAFS spectra for Co(II)/α-Al_2O_3 on the R ($1\bar{1}02$) plane. (a) Adsorption time of 6 days in parallel and perpendicular polarizations together with $Co(OH)_2$ as a reference. (b), (c) Different adsorption times (6 days, 1 hour) with or without a washing step in (b) parallel and (c) perpendicular polarizations.

The number of oxygen neighbors is also decreasing in the perpendicular polarization which can be explained by the complex dependence of the effective coordination number, determined in polarization-dependent measurements, with θ, the angle between the Co-X bond (directed along $\vec{r}$) and the electric field vector ($\overrightarrow{\varepsilon}$) [23] (Eq. (2))

$$N_{measured}(\theta) = \sum_{i=1}^{N_{real}} 3[\vec{\varepsilon}, \vec{r}]^2 = 3 \sum_{i=1}^{N_{real}} cos^2\theta$$

Eq. (2)

For a perpendicular orientation, θ tends toward 90° which leads to a decreased number of neighbors, both for Co and Oxygen.

Changing the deposition time (1 h vs. 6 days) and including a washing step do not change this conclusion since FTs shown on Figure 3-(b) (parallel polarization) and 3-(c) (perpendicular polarization) also demonstrate a surface-oriented precipitation of $Co(OH)_2$. One can note a slight increase of the number of Co 2nd neighbors with time in the parallel polarization (Figure 3-(b) and Table S1) suggesting a slight growth of the surface $Co(OH)_2$ phase from 1h to 6 days.

The interaction of cobalt(II) precursors on the R($1\bar{1}02$) plane was modeled by DFT according to the method reported in section 2.3., first simulating the grafting of one cobalt per unit cell (surface R, θ_{Co} = 1.0 nm^{-2}). The epitaxial positions depicted in Figure 2-a appeared to be favored, meaning that cobalt tends to occupy surface sites than should have been occupied by Al atoms in the bulk. The most favorable one (based on standard Gibbs free energy of adsorption $\Delta_rG°_{ads}$ calculations) corresponds to the occupation of one of the sites depicted in green in Figure 2-a. Its structure is depicted in Figure 4-a. A Gibbs free energy of adsorption $\Delta_rG°_{ads}$ of -259 kJ.mol$_{Co}^{-1}$ is calculated, in rather good agreement with the -234 kJ.mol$_{Co}^{-1}$ calculated on the (110) surface of γ-Al_2O_3 [25], in spite of the slight variation of the level of theory (dispersion corrections). The Co^{II} surface complex is octahedral, and its coordination

sphere is composed of one framework μ_2 oxygen (becoming μ_3 upon interaction with cobalt, d_{Co-O} = 1.95 Å), of two surface μ_1 OH groups (becoming μ_2-OH, average d_{Co-O} = 2.12 Å) and three water molecules (average d_{Co-O} = 2.22 Å). The total Co-O average bond length is d_{Co-O} = 2.14 Å, slightly higher than the experimental observations in EXAFS. As the longer Co-O contributions come from water coordinated molecules, this suggests that they are not dominant experimentally.

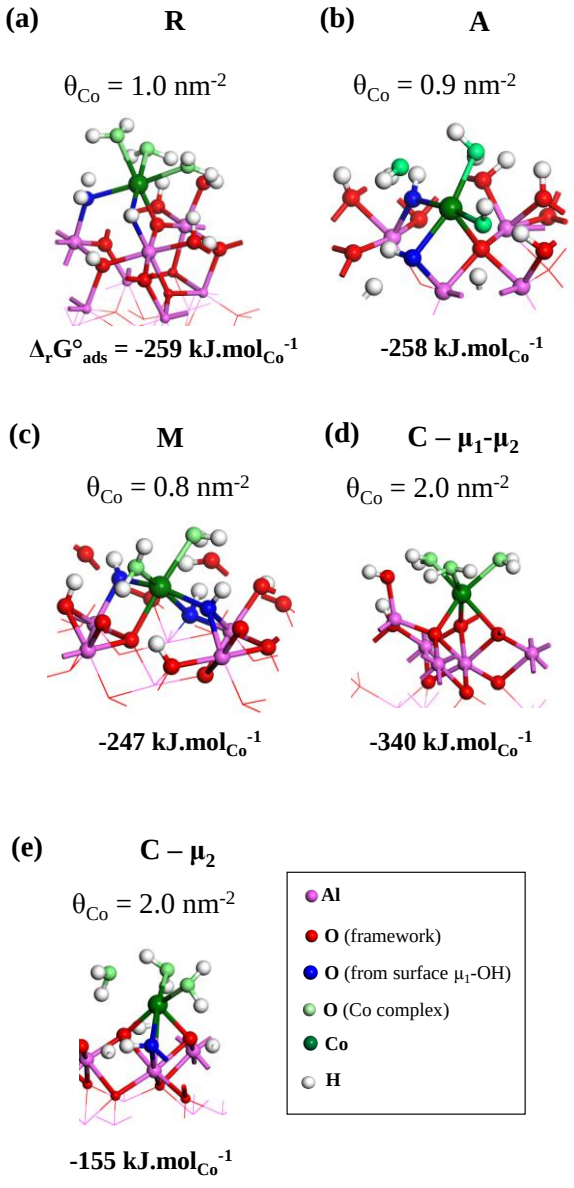

Figure 4. Perspective view of the coordination complexes obtained upon grafting of a single cobalt complex per unit cell for all surfaces modeled, together with the standard Gibbs adsorption free energy.

This motivates the simulation of the increase of Co coverage and of the condensation of cobalt (II) grafted complexes that shall result in i) the removing of such non-bridging water molecules, ii) the appearance of Co-Co proximity, as observed experimentally. Increasing the simulated Co coverage, several coordination modes were investigated at θ_{Co} = 1.99 nm^{-2}: (i) the increase of the coverage in dispersed complexes (Figure 5-a), (ii) the epitaxial growth by grafting the second cobalt complex on surface sites, and with two shared hydroxyl ligands with the first Co complex (Figure 5-b), (iii) apical coordination of the second complex, leading to an out-of-surface growth mode (Figure 5-c). The $\Delta_r G°_{ads}$ values show that the strength of the interaction is slightly depleted when increasing the coverage, and that all modes are competitive. The out-of-surface mode is slightly less stable than the two other ones, suggesting a preferred growth onto the surface. For the epitaxial growth mode (Figure 5-b), the Co-Co bond length in the dimer is of 3.02 Å, in reasonable agreement with experimental data (3.12-3.17 Å), together with an average Co-O bond length of 2.12 Å with a CN of 6. This bond length average remains slightly higher than the experimental one (2.04-2.09 Å).

The coverage was increased more, confirming the trends observed at θ_{Co} = 1.99 nm^{-2}. At θ_{Co} = 5.97 nm^{-2} (the highest surface coverage simulated on this surface, that already exceeds the coverage measured experimentally, see Figure 1), the most stable configuration obtained is depicted in Figure 5-d, and corresponds to the extension of the cobalt hydroxide-like chain, the third complexes of each chains (two chains per unit cell) being connected to the surface only thanks to the previous cobalt complex, plus an additional Co-O bond with a μ_1-OH underneath. On this surface coordination structure, two thirds of the cobalt atoms are octahedral or nearly octahedral (one longer Co-ligand bond), the last third being four-fold coordinated due to the desorption of the two excess water molecules that had been put on it

before geometry optimization. As they were ejected in the course of the optimization, a second structure minimization was performed by removing these from the system. A structure analysis leads to the average feature reported in Table S2. At such high coverage, the average Co-O length slightly decreases (2.10 Å) with respect to simulations performed at low coverage. This value is in good agreement with experimental observations. This confirms that water molecules are in minority in the coordination sphere of cobalt, hydroxyls being the dominant ligands. Notably, the calculations also suggest the presence of Co-Al proximity (2.85 Å) but at low CN (1.3) with respect to oxygen (5.3), likely explaining why they cannot be invoked from the experimental fit. A corollary of the coverage increase on the R surface, according to the grafting modes found by DFT, is a dramatic decrease of the Co-Co average bond length down to 2.52 Å.

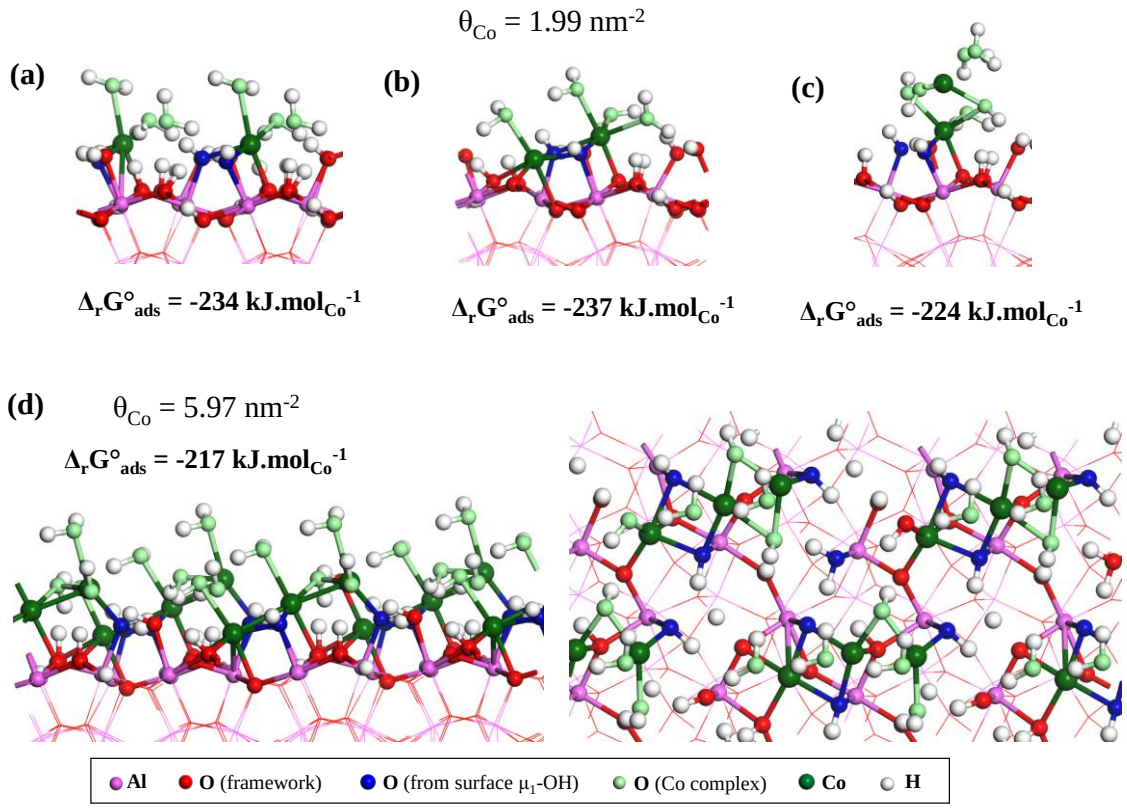

Figure 5. Surface complexes on the R orientation, and corresponding standard Gibbs adsorption free energy average by cobalt unit, according to various configurations: (a) two dispersed complexes, (b) epitaxil growth, (c) apical growth, for θ_{Co} = 1.99 nm^{-2} (two cobalt per unit cell). (d) Side (left) and top (right) views of the surface complexes on the R orientation for θ_{Co} = 5.97 nm^{-2} (six cobalt per unit cell).

This is likely due to the mismatch between the Co-O and Al-O bond lengths, that leads to short Co-O bonds when epitaxial growth takes place. Such a feature is not appearing experimentally, suggesting that the next growth steps will take place without further anchoring of the cobalt complexes on the surface. Thus, cobalt hydroxide layers may be grafted only by a few anchoring points on the R surface, so that in average, the specificity of the cobalt environment at the grafting point is not detected.

To go further, an analogy between the growth scheme and the structure of $Co(OH)_2$ layers can be drawn, similar as what was inferred for γ-Al_2O_3 [25]. Analyzing the symmetry of the surface deposit obtained at θ_{Co} = 5.97 nm^{-2}, and assuming that the growth of the cobalt hydroxide layer will follow the growth orientation dictated by the surface deposit, one obtains the layer orientation depicted in Figure S3. The angle between the layer grown from the deposit and the alumina surface is expected to be 60°, which should result in a higher perpendicular *versus* parallel contribution in GI-EXAFS. The opposite trend is observed experimentally, from which it can be concluded that the main growth mode does not follow the orientation dictated by the most stable surface deposit, and that likely a curvature of cobalt hydroxide layer shall take place, probably promoted by physisorption onto the R alumina surface due to van der Waals and electrostatic interactions.

3.2. Comparison of the R, A and M surfaces

Comparison of EXAFS results obtained on the R($1\bar{1}02$) plane with those on the A($11\bar{2}0$) and M($10\bar{1}0$) planes is shown on Figure 6 for long adsorption times (6 days). Fitting results are shown in Table S3. From qualitatively (EXAFS FTs) and quantitatively (fitting results) considerations, it can be safely concluded that the Co deposition mode on these three planes is very similar and leads to an oriented surface precipitation of $Co(OH)_2$ parallel to the surface demonstrated by the large polarization dependence of the peak assigned to Co-Co 2nd

neighbors at about 2.7 Å on Figure 6 (uncorrected for phase-shift) which correspond to a distance of 3.14-3.17 Å.

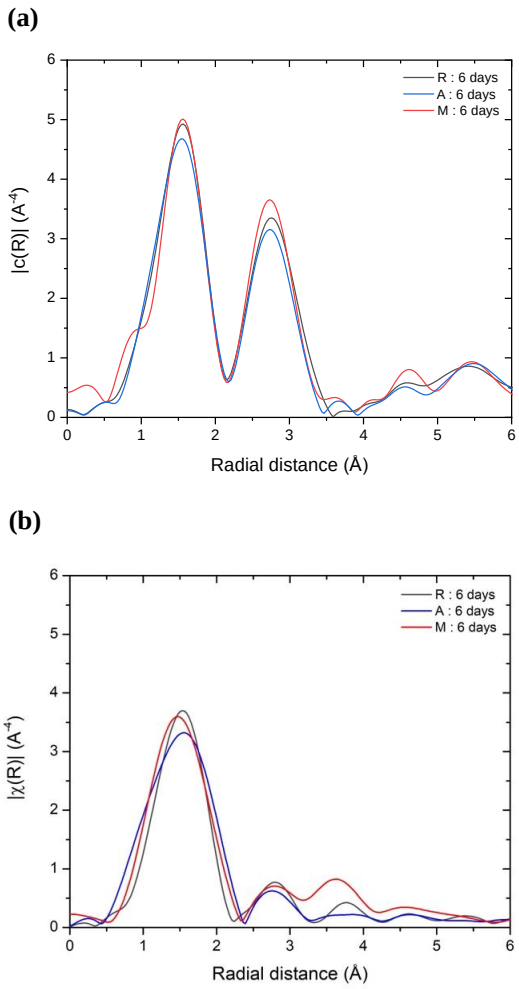

Figure 6. Fourier transforms (Δk = 3-8.5 $Å^{-1}$) uncorrected for phase shift of k^3-weighted Co K-edge EXAFS spectra for Co(II)/α-Al_2O_3 on the R ($1\bar{1}02$), A($11\bar{2}0$) and M($10\bar{1}0$) planes for long adsorption times (6 days). (a) Parallel polarization, (b) perpendicular polarization.

In a similar spirit as done for the R orientation, DFT calculations were performed to quantify the interaction strength and the geometry of possible surface deposits with the A and M surfaces, first for low Co coverage (Figure 4-b-c). $\Delta_r G°_{ads}$ values are highly similar with what was observed on the R surface, as well as the coordination chemistry of the mononuclear grafted surface complexes. At higher coverage, the surface-driven growth according to our calculations mode follows a rather messy process on surface A, with many competitive

grafting geometries, and $\Delta_r G°_{ads}$ values between -220 and -230 kJ.mol$_{Co}^{-1}$ at θ_{Co} = 5.60 nm^{-2}. Regarding the M orientation, the investigation of a loading increase depicts the ability of this surface to saturate with cobalt, with energetic features that are well maintained whatever the coverage ($\Delta_r G°_{ads}$ = -234 kJ.mol$_{Co}^{-1}$ at θ_{Co} = 16.18 nm^{-2}).

A structure analysis is proposed in Table S2 for the highest coverage modeled. In the coverage range investigated for the A and M surfaces, short (2.53-2.57 Å) and long (3.16-3.26, but also 3.67 Å) Co-Co distances co-exist. This disagreement with experiments is also reflected by the predicted orientations of the deposit-oriented growth mode, predicted at 25° and 30° for the A and M surfaces respectively, Figure S3, while experiments show that a parallel growth dominates. However, one notes that the perpendicular contribution of the M surface is graphically slightly higher than the one of the two other surfaces (despite a lower angle with respect to the R surface), which might be in link with the very good ability of this surface to reach high cobalt coverage with constant thermodynamic driving-force, as shown by DFT calculations.

Overall, the surface adsorption of Co(II) on the R ($1\bar{1}02$), A($11\bar{2}0$) and M($10\bar{1}0$) planes appears to follow a common mechanism characterized by a surface-driven growth of $Co(OH)_2$ oriented with respect to the surface (with an angle ranging from 25 to 60° depending on the surface) followed by a curvature of the hydroxide layer promoted by physisorption onto the alumina surface with van der Waals and electrostatic interactions.

3.3. Specific behavior of the C surface

EXAFS results obtained for Co(II) adsorption on the C(0001) plane leads to different results (Figure 7, and Table S4 for fitting results of the parallel polarization) as compared to the surfaces investigated previously. At short adsorption times (1 hour), fast surface precipitation of $Co(OH)_2$ is observed (Figure 7-(a)), rather similarly as what was observed for

the three previous surface orientations. The washing step does not appear to modify the nature of the surface precipitate except for a small decrease of the number of Co-Co 2nd neighbors (from 6 to 4). For such short adsorption times, the surface precipitation of $Co(OH)_2$ is also oriented since the perpendicular polarization do not show any contribution from Co-Co 2nd neighbors. These results differ from that obtained in a previous work [30] where the C(0001) plane appeared to be totally inert with respect to Ni(II) adsorption/precipitation. Such difference may be explained by a different adsorption pH (i.e. 7.0 for the Ni(II) case and 8.5 for the present case). A more basic pH will favor surface precipitation.

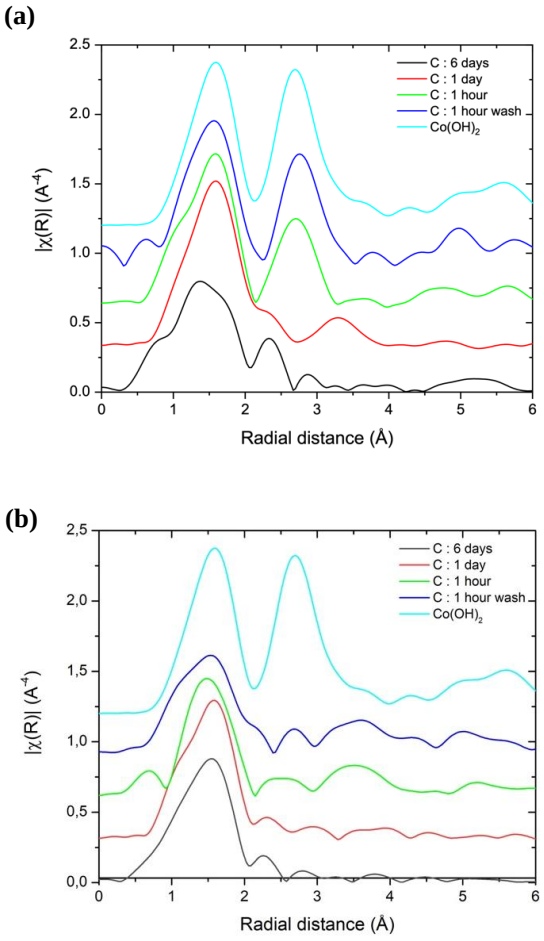

Figure 7. Fourier transforms (Δk = 3-8.5 Å^{-1}) uncorrected for phase shift of k^3-weighted Co K-edge EXAFS spectra for Co(II)/α-Al_2O_3 on the C(0001) plane for different adsorption times (1 hours vs. 6 days) with or without a washing step. (a) Parallel polarization, (b) perpendicular polarization.

Results are clearly different for longer adsorption times (1 day, 6 days, Figure 7) since the Co-Co second neighbors contributions are no longer dominant in both polarization

(parallel and perpendicular) suggesting a large structural evolution with time from 1 h to 1 day. The oxygen coordination number is rather high for 1 day in parallel polarization (7.2) which can also be explained by the $3\cos^2\theta$ dependence of the effective (measured) coordination numbers mentioned above. Hence, for a single neighbor, the coordination number can theoretically vary from 0 ($\theta = 90°$) to 3 ($\theta = 0°$). Hence, coordination numbers have to be taken here as qualitative and comparative guides among samples.

The most striking result on the C surface, with respect to other surface orientations, is the variation of the Co-Co distance as a function of time, accompanying the drop in second neighbor numbers. Whereas after 1 hour Co-Co is typical of cobalt hydroxide (3.17 Å), after 1 day it becomes much higher (3.89 Å), but it drops after 6 days (2.90 Å). This suggests the following mechanistic sequence:

- First, cobalt hydroxide layers are formed as precipitates parallel to the surface,
- Then, they dissolve and give rise to a surface deposit in a dispersed state, where the distance between cobalt species becomes larger
- Finally, a constrained deposit is formed, with a short Co-Co distance.

DFT calculations may give insight on the nature of such a constrained surface deposit obtained after long adsorption times. From a symmetry point of view, a significant difference of the C orientation with respect to all other investigated surfaces can already be seen from Figure 2. The expected epitaxial growth corresponds to an hexagonal symmetry, similar to the one of the cobalt hydroxide layers. Thus, the surface deposit-driven growth mode is expected to be parallel to the surface, but with possible direct coordination of cobalt (II) ions onto the surface, which is a major difference with respect to other surfaces. To quantify the feasibility of such an epitaxial cobalt hydroxide layer onto the C alumina surface, we simulated by periodic DFT the interaction of Co(II) precursors with the C-μ_1-μ_2 and C-μ_2 at low coverage ($\theta_{Co} = 2.00$ nm^{-2}). The behavior of these terminations appears to be very different: whereas the

C-μ_2 termination exhibits poor affinity for the cobalt precursor (-155 kJ.mol$_{Co}^{-1}$, Figure 4-e), the C-μ_1-μ_2 interacts much more strongly with cobalt than any other investigated surface (-340 kJ.mol$_{Co}^{-1}$, Figure 4-f). One specificity of the most favorable adsorption mode is to promote a dense network of hydrogen bonds between the three water molecules coordinated to cobalt, and the μ_1-OH groups of alumina. The grafted cobalt atom occupies a site that is at the same height with respect to the aluminum atom holding the μ_1-OH, although the geometry optimization slightly displaces it above the surface, due to longer Co-O bonds with respect to Al-O bonds. Conversely, on the C-μ_2 termination, cobalt lies on the row above all surface Al atom, weakening the interactions with the surface sites.

Thus, higher loadings were mainly computed for the C-μ_1-μ_2 termination. Figure 8 reports some of the optimized structures, for θ_{Co} = 8.11 nm^{-2} (4 Co per unit cell) and θ_{Co} = 14.19 nm^{-2} (7 Co per unit cell). The former corresponds to the saturation of the epitaxial sites (see Figure 2-d), the later corresponds to the saturation of all possible grafting site, although a 8th cobalt atom should have been hosted to fill all holes, but the $\Delta_r G°_{ads}$ values obtained with 8 Co per unit cell are prohibitively positive (not shown), even upon variation of the hydration level. This shows that a full cobalt-hydroxide like layer, where Al are incorporated, is submitted to a strong strain at the alumina surface. This can be assigned to the mismatch between the Co-O and Al-O bond lengths. At θ_{Co} = 8.11 nm^{-2}, where all the epitaxial sites are occupied, $\Delta_r G°_{ads}$ equals -253 kJ.mol$_{Co}^{-1}$, which reveals a much stronger interaction than any other surface in this range of cobalt coverage. This value is similar to the one obtained for R, A and M at the lowest investigated coverage. At saturation (θ_{Co} = 14.19 nm^{-2}), the $\Delta_r G°_{ads}$ value (-221 kJ.mol$_{Co}^{-1}$) is still competitive with the apical growth depicted in Figure 5-c. We can thus conclude that the filling of all epitaxial site is a favored process, with a clear driving force, and reaching saturation is feasible, which was not the case for other surface orientations (R, A and M). The structural analysis for the saturated surface model is proposed in Table S2.

A short Co-Co distance is recorded (2.45 Å), although shorter than the experimentally measured one (2.90 Å) after 6 days of adsorption. It co-exists with longer distances in the model, suggesting that our proposed model is probably not exactly representing the true configuration. However, the energetic specificity of the C surface quantified by DFT, together with the observation of short Co-Co distances when epitaxial growth is modeled, makes us confident in the conclusion according to which the C surface is the single α-alumina surface orientation (among those considered in the present work) able to lead to a constrained surface deposit stabilized by epitaxial growth at long contact times.

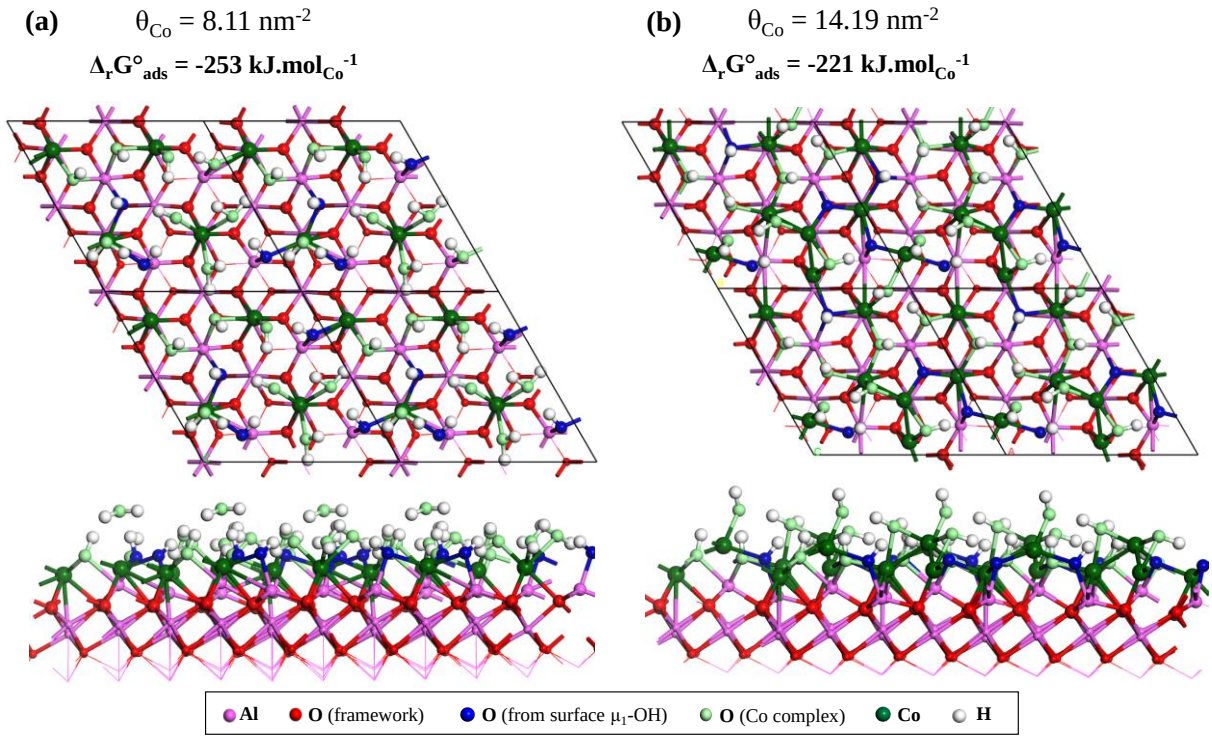

Figure 8. Top (top) and side (bottom) views of the surface structures optimized by DFT for the C-μ_1-μ_2 termination at (a) θ_{Co} = 8.11 nm^{-2} (b) θ_{Co} = 14.19 nm^{-2}.

4. CONCLUSIONS

In the present study, we investigate the interaction of cobalt (II) with alumina surfaces, which understanding is crucial for the optimization of a large set of industrially used

heterogeneous catalysts. α-alumina is chosen as a model system, opening the possibility to experimentally investigate independently the behavior of various surface orientations, contrary to poorly crystalline supports such as γ-alumina.

A surface-dependent interaction is demonstrated by grazing-incidence EXAFS at the Co K-edge, complemented by periodic DFT calculations. R, A and M surface orientations follow a similar behavior: the formation of cobalt hydroxide is observed, that grow parallel to the alumina surface. We propose that the $Co(OH)_2$ layers are grafted onto the surface by only a few anchoring points, that do not dictate the layer orientation with the surface at long distances (Figure 9).

The C surface behaves very differently. Whereas at short contact times (one hour) the same $Co(OH)_2$ precipitate is formed, it then disappears (one day and more) and gives rises to a constrained surface deposit with short Co-Co distances (2.90 Å). The specific behavior of the C surface can be assigned to the surface symmetry of this surface plane, prone to host an epitaxial plane of $Co(OH)_2$, interrupted by surface Al atoms that are not detected in EXAFS probably due to a large local surface disorder. The two kinetic regimes observed experimentally can be assigned as follows (Figure 9):

- First, at low contact time, the quicker process is the formation of cobalt hydroxide layers, that grow only with a few covalent anchorage points with the alumina support, but are likely in van der Waals plus electrostatic interaction with the surface, which explains a preferred parallel orientation detected in GI-EXAFS. This feature is common to all surface interactions. We propose the existence of grafting points although they are not experimentally detected, both on the basis of DFT calculations, and considering that in the present conditions, homogeneous precipitation of $Co(OH)_2$ is not expected to take place. These grafting points are, however, not as numerous as what our DFT calculations

would suggest, because we did not simulate explicitly the stabilization (likely very high) of a cobalt hydroxide layer grown parallel to the surface.

- At longer contact time, dissolution of the hydroxide surface layer is observed on the C surface followed by coordination of cobalt, with a gradual cobalt coverage increase, leading to a decrease of Co-Co distances. The fact that such a coordination takes longer than the independent growth of cobalt hydroxide may be assigned to the higher entropy loss of the cobalt complex upon immobilization at the surface, likely to increase the preexponential factor of the rate constant. Another explanation can be that the C surface needs to be of the C-μ_1-μ_2 type to be at the origin of a strong thermodynamic driving force for the coordination of cobalt. Should the C-μ_2 termination be more abundant, a reconstruction (possibly induced by cobalt itself) into the C-μ_1-μ_2 type will be necessary. This is likely at the origin of kinetic limitations.

The second step is not observed on the other surface orientations. DFT suggests that the grafting thermodynamic driving force is indeed lower, but we cannot exclude that kinetic limitations also contribute to the absence of evolution to the grafted state.

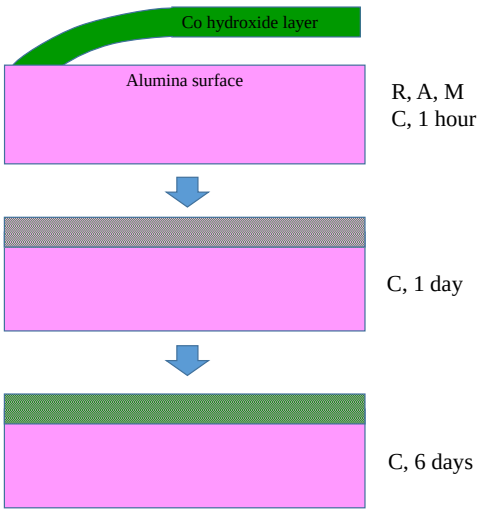

Figure 9. Scheme depicting the possible growth mode of cobalt deposits on the C surface from a cobalt hydroxide layer present on surfaces R, A et M whatever the adsorption time and on the C plane at short adsorption times only. After 1 day on the C Plane, a surface deposit in a dispersed state is formed

characterized by long Co-Co distances (3.89 Å), while for 6 days, a constrained surface deposit grows with short Co-Co distances of 2.90 Å in epitaxial relationship with the surface.

In terms of possible consequences on catalytic performances, the C surface is thus the most likely to give rise to poorly reducible species due to an epitaxial relationship between the surface and the constrained Co deposit. Hardly reducible species are to be avoided for applications in hydrotreating and Fischer-Tropsch.

Finally, an analogy has been made between the C surface of α-alumina [28] and the (111) surface of γ-Al_2O_3 [48, 49]. Should this analogy be followed in the case of interaction of alumina with cobalt (II) precursors, a specific interaction should be observed with the γ-Al_2O_3 (111) surface, that was not considered in previous theoretical works [25]. This could be a motivation for further experimental and computational investigations, as well as a lever to monitor catalytic performances from the tuning of the alumina support morphology.

Acknowledgements. CC thanks Dominique Costa (Chimie Paris Tech) and Kim Larmier (IFP Energies nouvelles) for discussion about the alumina surface models. The DFT calculations were performed using HPC resources from GENCI (Grant A0020806134) and the ENER440 cluster at IFP Energies nouvelles. We also acknowledge SOLEIL for provision of synchrotron radiation facilities (proposal 20160216) and we would like to thank Guillaume Alizon for assistance in using beamline SAMBA. This work was supported by the French National Research Agency within the framework of the ANR-14-CE08-0019 SLIMCAT project.

References

[1] P. Raybaud, H. Toulhoat, Catalysis by Transition Metal Sulphides, From Molecular Theory to Industrial Application, Technip, Paris, 2013.
[2] A.Y. Khodakov, Catal. Today 144 (2009) 251-257.
[3] H. Schulz, Appl. Catal. A 186 (1999) 3-12.
[4] F. Jiao, H. Frei, Angew. Chem. Int. Ed. 48 (2009) 1841-1844.
[5] B.S. Yeo, A.T. Bell, J. Am. Chem. Soc. 133 (2011) 5587-5593.
[6] X. Xie, Y. Li, Z.Q. Liu, M. Haruta, W. Shen, Nature 458 (2009) 746-749.
[7] J.L. Ewbank, L. Kovarik, C.C. Kenvin, C. Sievers, Green Chem. 16 (2014) 885.
[8] Z. Ferencz, E. Varga, R. Puskás, Z. Kónya, K. Baán, A. Oszkó, A. Erdőhelyi, J. Catal. 358 (2018) 118-130.
[9] G.L. Bezemer, J.H. Bitter, H.P.C.E. Kuipers, H. Oosterbeek, J.E. Holewijn, X. Xu, F. Kapteijn, A.J. van Dillen, K.P. de Jong, J. Am. Chem. Soc. 128 (2006) 3956-3964.
[10] J.P. den Breejen, P.B. Radstake, G.L. Bezemer, J.H. Bitter, V. Frøseth, A. Holmen, K.P. de Jong, J. Am. Chem. Soc. 131 (2009) 7197-7203.
[11] N.E. Tsakoumis, J.C. Walmsley, M. Ronning, W. van Beek, E. Rytter, A. Holmen, J. Am. Chem. Soc. 139 (2017) 3706-3715.
[12] P. Munnik, P.E. de Jongh, K.P. de Jong, J. Am. Chem. Soc. 136 (2014) 7333-7340.
[13] J.F. Lambert, M. Che, J. Mol. Catal. A 162 (2000) 5-18.
[14] F. Dumond, E. Marceau, M. Che, J. Phys. Chem. C 111 (2007) 4780-4789.
[15] K. Bourikas, C. Kordulis, J. Vakros, A. Lycourghiotis, Adv. Colloid Interface Sci. 110 (2004) 97-120.
[16] J.L. Paulhiac, O. Clause, J. Am. Chem. Soc. 115 (1993) 11602-11603.
[17] J.B. d'Espinose de la Caillerie, M. Kermarec, O. Clause, J. Am. Chem. Soc. 117 (1995) 11471-11481.
[18] L. Vandewater, G. Bezemer, J. Bergwerff, M. Versluijshelder, B. Weckhuysen, K. De Jong, J. Catal. 242 (2006) 287-298.
[19] P. Munnik, N.A. Krans, P.E. de Jongh, K.P. de Jong, ACS Catal. 4 (2014) 3219-3226.
[20] A. Jean-Marie, A. Griboval-Constant, A.Y. Khodakov, F. Diehl, C. R. Chimie 12 (2009) 660-667.
[21] W. Chu, P. Chernavskii, L. Gengembre, G. Pankina, P. Fongarland, A. Khodakov, J. Catal. 252 (2007) 215-230.
[22] A.K. Dalai, B.H. Davis, Appl. Catal. A 348 (2008) 1-15.
[23] M. Shirai, K. Asakura, Y. Iwasawa, Catal. Lett. 15 (1992) 247-254.
[24] S.N. Towle, J.R. Bargar, G.E. Brown, G.A. Parks, J. Colloid Interface Sci. 217 (1999) 312-321.
[25] K. Larmier, C. Chizallet, P. Raybaud, Angew. Chem., Int. Ed 54 (2015) 6824-6827.
[26] B.F. Ngouana Wakou, M. Corral Valero, P. Raybaud, J. Phys. Chem. C 122 (2018) 19560-19574.
[27] T. Yang, M. Ehara, Phys. Chem. Chem. Phys. 19 (2017) 3679-3687.
[28] C. Bara, A.-F. Lamic-Humblot, E. Fonda, A.-S. Gay, A.-L. Taleb, E. Devers, M. Digne, G.D. Pirngruber, X. Carrier, J. Catal. 344 (2016) 591-605.
[29] R.A. Garcia de Castro, J. Bertrand, B. Rigaud, E. Devers, M. Digne, A.-F. Lamic-Humblot, G. Pirngruber, X. Carrier, Chem. Eur. J. n/a (2020).
[30] A. Tougerti, I. Llorens, F. D'Acapito, E. Fonda, J.L. Hazemann, Y. Joly, D. Thiaudiere, M. Che, X. Carrier, Angew. Chem. Int. Ed. 51 (2012) 7697-7701.
[31] C. Bara, L. Plais, K. Larmier, E. Devers, M. Digne, A.-F. Lamic-Humblot, G.D. Pirngruber, X. Carrier, J. Am. Chem. Soc. 137 (2015) 15915-15928.

[32] S.N. Towle, J.R. Bargar, G.E. Brown Jr, G.A. Parks, J. Colloid Interface Sci. 187 (1997) 62-82.
[33] V. Briois, E. Fonda, S. Belin, L. Barthe, C. La Fontaine, F. Langlois, M. Ribbens, F. Villain, UVX 2010 - 10e Colloque sur les Sources Cohérentes et Incohérentes UV, VUV et X ; Applications et Développements Récents (2011) 41-47.
[34] B. Ravel, M. Newville, J. Synchrotron Rad. 12 (2005) 537-541.
[35] G. Kresse, J. Hafner, Phys. Rev. B 49 (1994) 14251-14269.
[36] G. Kresse, J. Furthmüller, Comput. Mat. Sci. 6 (1996) 15-50.
[37] J. Perdew, K. Burke, M. Ernzerhof, Phys. Rev. Lett. 77 (1996) 3865-3868.
[38] S. Grimme, J. Comput. Chem. 27 (2006) 1787-1799.
[39] T. Bucko, J. Hafner, S. Lebegue, J.G. Angyan, J. Phys. Chem. A 114 (2010) 11814-11824.
[40] G. Kresse, D. Joubert, Phys. Rev. B 59 (1999) 1758-1775.
[41] S.H. Vosko, L. Wilk, M. Nusair, Can. J. Phys. 58 (1980) 1200-1211.
[42] H.S.R. Gilson, M. Krauss, J. Phys. Chem. A 102 (1998) 6525-6532.
[43] V. Laget, S. Rouba, P. Rabu, C. Hornick, M. Drillon, J. Magn. Magn. Mater. 154 (1996) L7-L11.
[44] T.P. Trainor, P.J. Eng, G.E. Brown, I.K. Robinson, M.D. Santis, Surf. Sci. 496 (2002) 238-250.
[45] A. Tougerti, C. Méthivier, S. Cristol, F. Tielens, M. Che, X. Carrier, Phys. Chem. Chem. Phys. 13 (2011) 6531-6543.
[46] X.G. Wang, A. Chaka, M. Scheffler, Phys. Rev. Lett. 84 (2000) 3650-3653.
[47] Z. Łodziana, J.K. Nørskov, P. Stoltze, J. Chem. Phys. 118 (2003) 11179-11188.
[48] M. Digne, P. Sautet, P. Raybaud, P. Euzen, H. Toulhoat, J. Catal. 211 (2002) 1-5.
[49] M. Digne, P. Sautet, P. Raybaud, P. Euzen, H. Toulhoat, J. Catal. 226 (2004) 54-68.